

Electronic Energy Transfer from Metastable Argon ($4s\ ^3P_{2,0}$) to Xenon, Oxygen and Chlorine Atoms

BY DAVID L. KING,[†] LARRY G. PIPER[‡] AND DONALD W. SETSER*

Department of Chemistry, Kansas State University,
Manhattan, Kansas, U.S.A. 66506

Received 10th May, 1976

The rate constants for product channels arising from quenching of metastable argon ($^3P_{2,0}$) atoms by xenon, oxygen and chlorine atoms have been measured by observing product emission intensities in a discharge-flow apparatus. The xenon and chlorine atom cases provide interesting contrasts in the distribution of product states, although the total quenching rate constants are large and of similar magnitude. Quenching by xenon gives a broad distribution of exit Xe^* channels, but all are relatively close (≤ 0.25 eV) to the entrance channel in energy. Quenching by Cl atoms also gives a variety of products but the favoured channels are the $Cl^*(4s)$ states which are ~ 2.5 eV below the entrance channel. The difference in exit channel distributions reflects the presence of attractive potentials for $ArCl^*$, including the Ar^+Cl^- potential. Quenching by oxygen atoms provides a third contrast because the quenching is specific with one exit channel, $O(3p^3P)$, being favoured. Since this channel is 0.5 eV below the entrance channel, attractive potentials again must be important.

Detailed experimental characterization and even rudimentary theoretical understanding of electronic energy transfer processes involving atoms and small molecules are generally unavailable. If the initially excited species and the final products are well characterized states of atoms and, if Penning and associative ionization are not energetically allowed exit channels, the final products will be electronically excited states of the quencher with the excess energy appearing as translational energy of the departing atoms. Even for the simplest cases, the lack of information about excited state potential curves makes interpretation difficult.¹⁻² Studies from this laboratory have used the lowest excited (metastable) states of the rare gases as the initially excited species. Quenching of $Ar(^3P_2)$ by Kr^2 gives two $Kr(5p)^*$ levels as products; both are within 0.022 eV of the $Ar(^3P_2)$ entrance channel; a direct curve crossing in the potential well of the entrance channel adequately explains the results. For oxygen atoms only, the $O(3p^3P)$ state appears to be a product,³ but the rate constant is larger than for quenching by krypton in spite of the 0.56 eV energy defect. In this work^{4a} and in the companion paper,^{4b} additional studies of product-state distributions from quenching of metastable rare gas atoms by atoms will be summarized. These studies include results from $Ar^* + Cl$ and $Ar^* + Xe$ and further measurements and elaboration on the $Ar^* + O$ reaction. The Xe and Cl cases provide examples with a high density of exit channels for closed (Xe) and open shell (Cl) reagents. The Cl and O reactions illustrate the effects of attractive molecular potentials⁴ correlating with $Ar^* + Cl(O)$ and $Ar^+ + Cl^-(O^-)$.

The results are based upon analysis of the emission intensities from the isolated reaction of the metastable $Ar(^3P_{2,0})$ atoms with added reagent to obtain rate constants

[†] present address, Amoco Oil Co. R & D, Amoco Research Center, P.O. Box 400, Naperville, Illinois 60540, U.S.A.

[‡] present address, Physical Sciences Inc., 30A Commerce Way, Woburn, Mass. 01801, U.S.A.

for formation of individual product states. The work of this paper is based upon observations from 1000-200 nm, while the accompanying paper describes emission studies in the vacuum ultraviolet. Thus, emission from the entire range of excitation [up to 11.55 eV for $\text{Ar}(^3P_2)$ or 11.72 eV for $\text{Ar}(^3P_0)$] is covered. Line width measurements ^{4b, c} of the vacuum u.v. resonance lines for Cl^* and O^* give an estimate of the translational energy of the resonance states. We can therefore distinguish direct excitation, which must release large amounts of translational energy, from cascade excitation, which gives nearly thermal Doppler line profiles.

Atom-atom electronic energy-transfer usually involves one or more crossings or avoided crossings of potential-energy surfaces. Assignment of the symmetries of the initial and final states must include consideration of the total angular momentum quantum number, J , in addition to term values. Thus, entrance channels correlating with $\text{Ar}(^3P_2)$ or $\text{Ar}(^3P_0)$ are not necessarily of the same symmetry and may not lead to the same final product channels even in the absence of energy restrictions. Approximate correlation diagrams are used to aid in interpreting the distributions of product channels for these reactions.

For systems in which many product levels are populated ($\text{Ar}^* + \text{Cl}$, $\text{Ar}^* + \text{Xe}$), comparison of the experimental and statistical distributions of product channels is of interest. Such analyses have been done for reactive ^{5, 6} and inelastic processes ⁷ of atom plus diatomic or polyatomic systems. The atom-atom case is inherently simpler, since energy must appear either in translation or electronic excitation. Thus, the analysis of these systems by surprisal method is in essence a measure of the translational energy disposal following the inelastic collision.

EXPERIMENTAL

The room temperature discharge-flow reactor used for the present studies has been described previously.² Argon metastables were produced in argon bath gas at 0.5-10 Torr by flowing purified argon through a cold hollow-cathode discharge. The electrodes for the discharge were made from rolled Ta foil and were operated at 220 V and ~ 5 mA. The total concentration of argon metastables has been measured previously to be $\sim 10^{10}$ - 10^{11} cm^{-3} , depending on the geometry of the apparatus; the lower energy metastable predominates ($^3P_2 : ^3P_0 \cong 7:1$, dependent somewhat upon operating conditions). The quencher gas is introduced approximately 5 cm beyond the downstream (negative) electrode and mixes concentrically with the argon metastables. Light emitted from the mixing zone is observed normal to the flow direction. The majority of the experiments employed a 0.75 m Jarrel Ash monochromator fitted with an EMI 9558QA photomultiplier (S-20 response) and SSR photon counting rate meter. The spectrometer-photomultiplier combination was calibrated with a quartz iodine lamp. Some of the Cl^* emissions far in the red were measured with a 0.33 m McPherson monochromator equipped with a RCA 7102 (S-1 response) phototube and a picoammeter (Keithley Instruments, model 417). This latter system was also calibrated with the quartz-iodine lamp.

Production of Cl and O atoms was achieved by microwave dissociation of dilute mixtures (3-10 %) of Cl_2 or O_2 in Ar or He. The percent chlorine dissociation, 15-20 %, was determined by monitoring the fractional decrease of the Cl^*_2 continuum emission at 258 nm [produced by $\text{Ar}(^3P_{2,0}) + \text{Cl}_2$]⁸ upon turning on the microwave discharge. Determination of the % oxygen dissociation was less straightforward, since $\text{Ar}(^3P_{0,2}) + \text{O}_2$ does not give any O^*_2 emission. Therefore, in a separate experiment the argon flow was replaced by He and the decrease of $\text{O}^*_2(A-X)$ emission from $\text{He}(2^3S) + \text{O}_2$ ⁹ was measured upon turning on the microwave discharge. These latter measurements indicated an O_2 dissociation of 45-50 %.

Scattered light from the microwave discharge was a serious problem for the chlorine-atom experiments, because several of the atomic chlorine lines were the same as those produced by the $\text{Ar}(^3P_{2,0}) + \text{Cl}$ reaction. To alleviate this problem several remedies were adopted,

including installation of light traps, painting the chlorine line, and shielding the entrance slit of the monochromator by black cloth. Under such conditions, blank runs with the microwave discharge on and metastable discharge off produced no measurable chlorine atom emission.

For the Xe and Cl quenching experiments, emission measurements were carried out for a pressure range of 1-5 Torr in the mixing zone. No obvious relaxation effects among the Cl($4p$) levels were seen other than reduction of the overall signal level because of lower argon metastable atom concentration at the extreme ends of the pressure range. For this reason the Cl* intensities reported here were obtained for pressures of ~ 1 -2 Torr in the mixing zone, which gave highest signal levels. In contrast, the Xe* emission intensities were markedly pressure dependent and it was necessary to extrapolate to zero pressure to assign initial product channels. The relatively slow quenching of O($3p^3P$) to O($3p^5P$) by argon has been noted³ before; thus, the Ar($^3P_{2,0}$)+O experiments were done at 1 Torr and extrapolation to lower pressure was not necessary. Further work with Cl* is needed to decide whether collisional relaxation by Ar is truly inefficient or whether the relaxation effects are not easily observed from monitoring the broad population distribution of the Cl($4p$) levels.

RESULTS

Ar($^3P_{2,0}$)+Xe

Fig. 1 is an energy diagram for xenon; the observed transitions are summarized in the figure captions. The observed spectrum contained over 150 lines which were

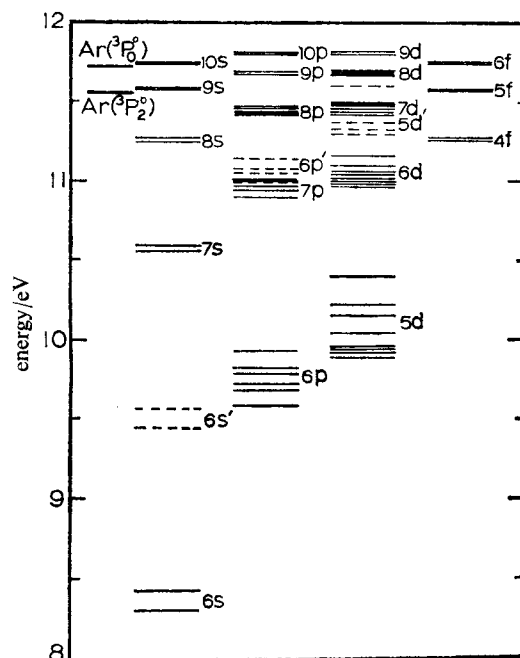


FIG. 1.—Energy level diagram for Ar($^3P_{2,0}$) and excited states of Xe below 11.80 eV. The dotted lines denote the primed configurations. The individual xenon states of each configuration are identified in tables 1 and 2. The following sets of transitions were studied: Ar(3P_2) excitation ($7d-6p$, $8p-6s$, $9s-6p$, $5f-5d$, $5f-6s$, $5d'-6p$); Ar(3P_0) excitation ($8d-6p$, $9p-6s$, $10s-6p$, $6f-5d$, $6f-5s$). Cascade induced populations ($6p'-6s'$, $6p'-6s$, $8s-6p$, $4f-6s$, $7p$, $6p-6s$, $6d-6p$). No emission was observed from the $7s'$ (11.97 eV), $11s$ (11.85 eV), $10p$ or $9d$ levels. For the higher sets of configurations all of the levels could not be shown on the scale of this diagram, *i.e.*, all f and d configurations have 8 levels and all p configurations have 6 levels.

assigned according to Striganov and Sventitskii.¹⁰ Transitions were observed from virtually all of the xenon levels which lie below the $\text{Ar}(^3P_{2,0})$ energy, although much of this emission results from radiative cascade from the higher levels that were excited directly by the metastable argon atoms. The assignment of primary excitation channels to the two different metastable species was done primarily on the basis of conservation of energy, *i.e.*, emissions from Xe levels above 11.6 eV were assigned to excitation by $\text{Ar}(^3P_0)$. The assignments decided on this basis were confirmed by varying the $^3P_2/^3P_0$ metastable ratio and noting the change in relative Xe* emission intensities.

For most of the states excited in the primary process, radiative transitions to only one of the several allowed sets of lower configurations were observed. However, all important transitions to the levels of that one lower configuration were studied except for the $5f-5d$ and possibly the $5d'-6p$ transitions. In order to correct the observed transitions for radiative branching to the configurations that were not observed (because of the restricted wavelength range), average branching ratios were calculated (see Appendix), because experimental branching ratios are available only

TABLE 1.—EXCITATION OF XENON LEVELS BY $\text{Ar}^*(^3P_0)$

level	E/eV	$\Delta E/\text{eV}^a$	k_{rel}^b	$(k_{\text{rel}}/g)^c$	$k^d/10^{11} \text{ cm}^3 \text{ molecule}^{-1} \text{ s}^{-1}$
$8d[{}^3_2]_1^0$	11.739	-0.016	0.04	0.01	0.08
$8d[{}^5_2]_3^0$	11.700	0.023	1.00 ^b	0.14	2.12
$8d[{}^5_2]_2^0$	11.696	0.027	0.91	0.18	1.93
$8d[{}^7_2]_3^0$	11.690	0.033	1.40	0.20	2.97
$8d[{}^7_2]_2^0$	11.690	0.033	1.40	0.28	2.97
$8d[{}^1_2]_1^0$	11.683	0.040	0.33	0.11	0.70 ₅
$8d[{}^3_2]_4^0$	11.682	0.041	2.52	0.28	5.34
$8d[{}^1_2]_0^0$	11.670	0.053	0.32	0.32	0.67
					16.78 ₅
$6f[{}^7_2]_{3,4}$	11.750	-0.027	0.71	0.04	1.51
$6f[{}^5_2]_2$	11.748	-0.025	0.15 ₆	0.03	0.33
$6f[{}^5_2]_3$	11.748	-0.025	0.50	0.07	1.05
$6f[{}^9_2]_4$	11.747	-0.024	0.64	0.07	1.36
$6f[{}^9_2]_5$	11.747	-0.024	0.99	0.09	2.10
$6f[{}^3_2]_{2,1}$	11.746	-0.023	1.17	0.15	2.47
					8.82
$9p[{}^1_2]_0$	11.690	0.033	0.18 ₇	0.19	0.39 ₅
$9p[{}^3_2]_2$	11.678	0.045	0.39	0.08	0.83
$9p[{}^3_2]_1$	11.675	0.048	0.21	0.07	0.45
$9p[{}^5_2]_3$	11.671	0.052	0.38	0.05	0.80
$9p[{}^5_2]_2$	11.668	0.055	—	—	—
$9p[{}^1_2]_1$	11.663	0.060	0.23	0.08	0.49
					2.96 ₅
$10s[{}^3_2]_1^0$	11.752	-0.029	0.23	0.08	0.49 ₅
$10s[{}^3_2]_2^0$	11.748	-0.025	0.44	0.09	0.93
					1.42 ₅

^a Energy defect relative to $E(\text{Ar}^*^3P_0) = 11.723 \text{ eV}$; ^b excitation rate constant relative to the $8d[{}^5_2]_3$ level; this level was selected for normalization because the $7d[{}^5_2]_3$ level was used for table 2. Note, however, that the $8d[{}^5_2]_3$ level is not the most favoured exit channel; ^c the relative excitation rate constant divided by the statistical weight, $g = 2J+1$; ^d total excitation rate constants based upon assumption that all quenching of $\text{Ar}^*(^3P_0)$ leads to Xe^* ; $k_Q(^3P_0) = 30 \times 10^{-11} \text{ cm}^3 \text{ molecule}^{-1} \text{ s}^{-1}$. See text for discussion of this assumption, which is questionable for $\text{Ar}(^3P_0)$.

for a few states.¹¹ In addition, corrections for collision-induced cascade were made by extrapolating the pressure-dependent relative populations to zero pressure.

The excitation rate constants for the individual levels were calculated from the product of the fraction of total excitation into a given level times the total quenching rate constant, which is $1.8 \times 10^{-10} \text{ cm}^3 \text{ molecule}^{-1} \text{ s}^{-1}$ and $3.0 \times 10^{-10} \text{ cm}^3 \text{ molecule}^{-1} \text{ s}^{-1}$ for $\text{Ar}(^3P_2)$ and $\text{Ar}(^3P_0)$, respectively.¹² This assumes that all quenching results in electronic excitation of xenon. The relative and absolute excitation rate constants for the various levels of xenon are given in tables 1 and 2 for $\text{Ar}(^3P_0)$ and $\text{Ar}(^3P_2)$.

TABLE 2.^c—EXCITATION OF XENON STATES BY $\text{Ar}^*(^3P_2)$

level	E/eV	$\Delta E/\text{eV}^a$	k_{rel}^b	$(k_{\text{rel}}/g)^c$	$k^d/10^{-11} \text{ cm}^3 \text{ molecule}^{-1} \text{ s}^{-1}$
$7d[^5_2]_3^o$	11.497	0.051	1.0 ^b	0.14	2.39
$7d[^3_2]_2^o$	11.496	0.052	0.74	0.15	1.77
$7d[^3_2]_1^o$	11.495	0.053	0.33	0.11	0.78
$7d[^5_2]_2^o$	11.490	0.058	0.94	0.19	2.25
$7d[^7_2]_3^o$	11.487	0.061	0.68	0.10	1.63
$7d[^7_2]_1^o$	11.46	0.09	0.50	0.06	1.19
$7d[^1_2]_{10}^o$	11.44	0.11	0.10	0.10	0.24
$7d[^1_2]_{11}^o$	11.42	0.13	0.12	0.04	0.28
					10.53
$5f[^7_2]_{3,4}$	11.582	-0.034	0.31	0.02	0.75
$5f[^5_2]_2$	11.580	-0.032	0.24	0.05	0.58
$5f[^5_2]_3$	11.580	-0.032	0.29	0.04	0.70
$5f[^5_2]_{14}$	11.577	-0.029	0.24	0.03	0.58
$5f[^9_2]_{15}$	11.577	-0.029	0.36	0.03	0.87
$5f[^3_2]_2$	11.576	-0.028	0.13 ₆	0.03	0.32 ₅
$5f[^3_2]_{11}$	11.575	-0.027	0.13	0.04	0.31
					4.12
$8p[^1_2]_0$	11.475	0.073	0.04 ₉	0.05	0.11 ₇
$8p[^3_2]_2$	11.452	0.096	0.20	0.04	0.48
$8p[^3_2]_{11}$	11.448	0.100	0.13 ₄	0.04 ₅	0.32
$8p[^5_2]_3$	11.439	0.109	0.11 ₁	0.02	0.28
$8p[^5_2]_2$	11.434	0.114	0.02	0.004	0.04 ₆
$8p[^1_2]_{11}$	11.425	0.123	0.14	0.05	0.33
					1.57
$9s[^3_2]_1$	11.583	-0.035	0.08	0.03	0.19
$9s[^3_2]_2$	11.580	-0.032	0.21	0.04	0.50
					0.69
$5d'[^5_2]_3$	11.375	0.173	0.13 ₄	0.02	0.32
$5d'[^3_2]_2$	11.34	0.21	0.30	0.06	0.71
$5d'[^5_2]_2$	11.30	0.25	0.02	0.004	0.04 ₃
					1.07

^a Energy defect relative to $E(\text{Ar}^*^3P_2) = 11.548 \text{ eV}$; ^b excitation rate constant relative to the $7d[^5_2]_3$ level which is the favoured exit channel; ^c relative excitation rate constant divided by statistical weight of the state, $g = 2J + 1$; ^d excitation rate constants based upon assumption that all quenching of $\text{Ar}^*(^3P_2)$ leads to excitation of Xe^* ; $k_Q(^3P_2) = 18 \times 10^{-11} \text{ cm}^3 \text{ molecule}^{-1} \text{ s}^{-1}$; ^e see text for discussion of the possible role of the $6p'$ levels.

The relative excitation rates are included, because for $\text{Ar}(^3P_0)$ excitation the total quenching rate and observed excitation rate may not necessarily be the same, as shown by the following experiment. The ratio of the densities of $\text{Ar}(^3P_2)$ and $\text{Ar}(^3P_0)$ was measured by absorption spectroscopy and compared to the ratio of the

Xe* emission intensities assigned to excitation by the two metastables. The intensity from $\text{Ar}^*(^3P_0)$ was significantly smaller than would be expected based upon the relative densities of the two metastables and their respective quenching rate constants. It is not clear, however, whether this effect arises from faulty radiative cascade corrections used to obtain total emission intensities, from more efficient collisional quenching of the longer-lived, higher-excited xenon states by argon bath gas, from quenching mechanisms other than direct transfer of electronic energy to xenon, or from excitation by $\text{Ar}(^3P_0)$ of some of the same Xe* as by $\text{Ar}(^3P_2)$. We suspect that the latter is the main effect. Since the density of $\text{Ar}(^3P_2)$ greatly exceeds that for $\text{Ar}(^3P_0)$, the excitation of the same Xe* levels by $\text{Ar}(^3P_2)$ and $\text{Ar}(^3P_0)$ will not seriously affect the product assignment for $\text{Ar}(^3P_2)$, even though all emissions originating from Xe* below $E(\text{Ar}, ^3P_2)$ were assigned to $\text{Ar}(^3P_2)$ in the present analysis of the data.

The relative rate constants (table 2) for $\text{Ar}(^3P_2)$ excitation of the $7d$, $5f$, $8p$ and $9s$ levels of Xe should be reliable. However, the $5d'$ rate constants may be less accurate since the cascade problem was not treated for this set of states; any error in excitation rate constants for the $5d'$ levels will not affect the relative rate constants of the $7d$, $5f$, $8p$ or $9s$ levels by more than 10-20%. Some of the particular difficulties encountered in the rate constant assignments are discussed below.

(i) Assignment of the $7d$ and $5f$ levels: emission from these levels was too strong to arise via radiative cascade from the $6f$ or $8d$ levels which are produced by $\text{Ar}(^3P_0)$. Also, the approximate branching ratio calculations indicate that $6f-7d$ and $8d-5f$ radiative transitions account for only a small fraction of the total transition probability from the $6f$ and $8d$ levels. Thus these rate constants are unambiguous.

(ii) Assignment of the $9s$ and $8p$ levels: the relative fractions of $\text{Ar}(^3P_0)$ and $\text{Ar}(^3P_2)$ were varied at fixed pressure and bulk flow rate to show that the Xe($9s$ and $8p$) levels were produced predominantly by direct reaction rather than by radiative cascade from the $9p$ and $8d$ levels. The ratio of 3P_0 to 3P_2 was lowered by more than a factor of 3 by a threefold increase in the distance between the discharge and observation region. No change was observed in the relative populations of the $9s$ and $8p$ levels, whereas the $9p$, $8d$ and $6f$ level populations were greatly reduced. Collisional transfer from Xe($7d$ or $5f$) was shown to be unimportant because the $9s$ and $8p$ levels were more strongly quenched with increasing argon pressure than were the $7d$ or $5f$ levels.

(iii) Assignment of the $5d'$ levels: the evidence supporting primary excitation for the Xe($5d'$) levels was the same as just mentioned for Xe($9s$ and $8p$); furthermore, radiative cascade from $6f$ would violate the selection rules of the $J_c - 1$ scheme (although this alone is not a conclusive argument, see below).

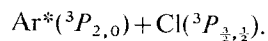
(iv) Levels populated by radiative cascade: emission was observed from the $8s$, $6p$, $6p'$, $7p$, $6d$ and $4f$ levels. In a qualitative study in the vacuum ultraviolet, emission has been observed from $6s$, $6s'$, $7s$ and $5d$ states.^{4c} These levels are most likely populated by radiative cascade from higher levels, although direct excitation by $\text{Ar}(^3P_2)$ cannot be ruled out definitively. The $\text{Ar}^* + \text{Xe}$ system, in contrast to the $\text{Ar}^* + \text{Cl}$ system, does not have strongly bound potential curves crossing the entrance channel which would allow a coupling of the entrance channel with these exit channels of large energy defect (≥ 0.4 eV). Radiative transitions populating the $6p$ and $5d$ levels were balanced in intensity by radiation out of the $6p$ levels (most of the $5d$ levels may radiate only to the $6p$ levels). Clearly, these levels must be populated by radiative cascade. Since the $6p$ and $5d$ levels are excited by radiative cascade, it is probably safe to assume that the lower lying $6s$ and $6s'$ states are excited by radiative cascade also. Even if there is direct excitation of the $7s$, $8s$, $7p$, $6d$ and $4f$ levels, the

rate constants in table 2 will not be affected by $> 10\%$ because the observed emission from these levels was weak in relation to the similar transitions from manifolds of higher principal quantum number.

(v) Radiative cascade to the Xe($6p'$) levels: the Xe($6p'$) set of levels, which probably are excited via radiative cascade (see above), had a zero-pressure population roughly twice that of Xe($5d'$), as judged by comparing the $5d'-6p$ and $6p'-6s$ and $-6s'$ emission intensities. According to the J_c-1 coupling scheme, the only allowed radiative transitions to the $6p'$ levels are from the $5d'$ levels. Thus we were tempted to add the $6p'$ population to that of the $5d'$ levels in assigning rate constants. However, transition probability calculations showed that if the major radiative pathway from the $5d'$ levels were transitions to the $6p'$ levels, the $5d'$ levels should have a lifetime of $\sim 1 \mu s$. Since Allen *et al.*¹³ tentatively assigned a lifetime of 150 ns to the $5d'$ levels, the major radiative pathway may be to levels other than $6p'$. The $6p$ levels are likely possibilities since transitions from Xe($5d'$) to the ground state Xe are dipole forbidden. This is consistent with the relatively strong Xe($5d'$ to $6p$) transitions which were observed in our work. Since the $\Delta J_c = 0$ selection rule may not be rigorous for $d-p$ transitions,¹⁴ radiative cascade from the $7d$ and $8d$ may also contribute to the $6p'$ population. Since the origin of the $6p'$ emission was uncertain, the populations of the $6p'$ levels were not added to any other levels. The intensities from these levels are sufficiently small such that neglect of this emission could introduce $\leq 15\%$ error in the relative excitation rates of all but the $5d'$ levels. If all of the $6p'$ populations originated from radiative cascade from the $5d'$ levels, these rate constants would be enhanced by a factor of 2 relative to those in table 2.

The assignment of the Ar(3P_0) primary excitation rate constants to the $8d$, $6f$, $9p$ and $10s$ states of xenon is straightforward because higher levels of xenon are absent and radiative cascade is not significant. Since the Xe($10s$ and $9p$) levels were more rapidly quenched by increasing argon pressure than the Xe($8d$ and $6f$) levels, the Xe($10s$ and $9p$) levels were not produced by collisional cascade from Xe($8d$ and $6f$). As already mentioned, there may be quenching pathways for Ar(3P_0) in addition to formation of the Xe* states shown in table 1.

The complexity of the xenon spectrum precludes the possibility of a detailed analysis of the collisional quenching of higher-excited xenon levels by ground-state argon. However, our data are in qualitative agreement with the suggestion that quenching cross sections for some Xe* states may be as large as several hundred square ångströms.¹³ The steady state population of the $6p'$ level seems to increase the most from collisional quenching of the Xe* levels. The $7p$ levels retained a fairly constant population, relative to all other Xe* levels, from 0.3-9 Torr. Emission from the $4f$ levels also was enhanced at higher pressures. The remaining levels, with the possible exception of the $6d$ levels which were observed only at low pressure, decreased in population as the pressure was increased. Little change was observed in the populations of J -state levels of a manifold; however, the two upper levels of the $6p$ manifold, $6p(\frac{1}{2})_0$ at 9.93 eV and $6p(\frac{3}{2})_2$ at 9.82 eV, were enhanced at higher pressure relative to the lower levels of this configuration. One consequence of the secondary collision processes is that formation of the 1P_1 and 3P_1 resonance states of xenon is enhanced at higher pressures, the former a result of the collisional cascade into the Xe($6p'$) levels, and the latter from collisional cascade into the $6p(\frac{1}{2})_0$ state, which mainly radiates to Xe(3P_1).



The energy levels for Cl are shown in fig. 2. The quenching of Ar(3P_0) will be considered first. The $3s^23p^44p(^2P^\circ)$ and the $3s^23p^45p(^4P^\circ$ and $^4D^\circ)$ levels lie

significantly higher in energy than $\text{Ar}(^3P_2)$; thus, emission from these levels must arise from interaction with $\text{Ar}(^3P_0)$. Some emission from the $^2P^\circ$, $^4P^\circ$ and $^4D^\circ$ levels is to the $\text{Cl}(4s^2P_J$ and $^4P_J)$ levels in the 400-500 nm region and is readily observable. Since transitions from these upper levels also occur to various $\text{Cl}(5s$ and $3d)$ levels, the observed emission intensity must be corrected for branching (see Appendix) before absolute formation rate constants can be established. To obtain absolute rate constants the Cl^* intensities (corrected for branching) from a $\text{Ar} + \text{Cl}_2 + \text{Kr}$ mixture, in which the $\% \text{Cl}_2$ dissociation was measured, were compared with the

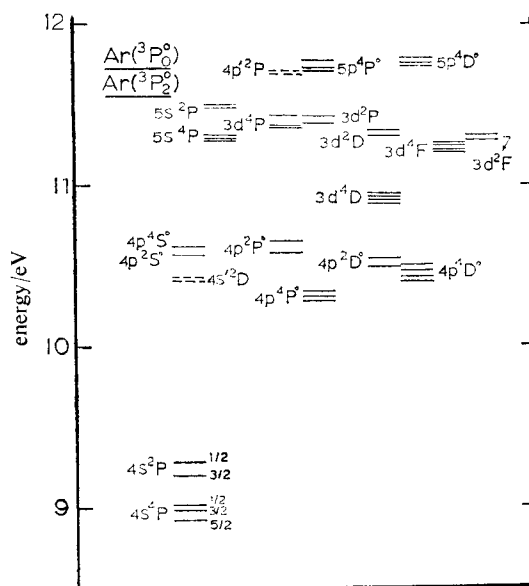


FIG. 2.—Energy level diagram for $\text{Ar}(^3P_{0,2})$ and excited states of chlorine atoms. The $4p'$, $5p$, and $4p$ manifolds were studied by observing transitions to the $4s$ levels. Transitions from $4s$, $4s'$, $5s$ and $3d$ were observed in the vacuum ultraviolet, see the accompanying paper. The ordering of the J levels is normal for the Cl^* states, *i.e.*, largest J is lowest in energy.

Kr^* emission intensity. The Kr^* and Cl^* intensity ratio, the Kr and Cl concentration ratio, the Kr^* excitation rate constant² and the $\text{Ar}(^3P_2)$ to $\text{Ar}(^3P_0)$ ratio (7:1 as measured by atomic absorption) are required to obtain the rate constants of table 3. All of these measurements were done under conditions such that the metastable atom concentrations were not significantly reduced; hence, the ratio of $\text{Ar}(^3P_2)$ to $\text{Ar}(^3P_0)$ was not altered by the addition of the $\text{Ar} + \text{Cl} + \text{Cl}_2$ mixture. Many of the emission lines originate from the Cl^* levels slightly higher (up to 750 cm^{-1}) than the $\text{Ar}(^3P_0)$ energy, which requires conversion of the initial translational collision energy to electronic energy in the products. Surprisingly, emissions from the $\text{Cl}(5p^4P^\circ)$ manifold show preference for $J = \frac{3}{2}$ over $J = \frac{5}{2}$, which are 0.013 eV endoergic and 0.009 eV exoergic, respectively. The data show no strong preference for the $5p$ quartet states relative to the $4p'$ doublet states, despite the change in core configuration required for formation of the latter. This conclusion, however, is strongly dependent upon the reliability of the calculation branching ratios (see Appendix). The observed $4p'-4s$ emissions actually were weaker than transitions from the $5p$ levels, but the calculated branching ratios (which do not include effects caused by changes in core

configurations) indicated that the $4p'$ - $5s$, $4s'$ and $3d$ transitions actually were stronger than those to the $4s$ levels.

The remaining atomic chlorine levels lie below the $\text{Ar}(^3P_2)$ energy and can be produced from either $\text{Ar}(^3P_2)$ or $\text{Ar}(^3P_0)$. Based upon the strong favouring of the $\text{Cl}(4s)$ states as exit channels rather than $\text{Cl}(5s, 3d, 4p)$, *vide infra*, and upon the 7 : 1 ratio of $\text{Ar}(^3P_2)$ to $\text{Ar}(^3P_0)$, all Cl^* emission from levels below 11.55 eV was assigned as $\text{Ar}(^3P_2)$ excitation. This assumption will result in little error for the $\text{Ar}(^3P_2)$ rate

TABLE 3.—RATE CONSTANTS FOR $\text{Ar}(^3P_0)$ +CHLORINE ATOMS ^a

level	energy/eV	$\Delta E/\text{eV}$ ^b	k_{rel} ^c	(k_{rel}/g)	rate constant/ $10^{-11} \text{ cm}^3 \text{ molecule}^{-1} \text{ s}^{-1}$
$5p$ $^4P_{3/2}^{\circ}$	11.714	0.009	0.24	0.04	0.051
$^4P_{1/2}^{\circ}$	11.737	-0.013	1.0	0.25	0.216
$^4P_{3/2}^{\circ}$	11.775	-0.051	0.018	0.009	0.004
					0.271
$5p$ $^4D_{3/2}^{\circ}$	11.745	-0.021	0.76	0.095	0.165
$^4D_{1/2}^{\circ}$	11.757	-0.033	0.10	0.017	0.022
$^4D_{5/2}^{\circ}$	11.818	-0.094	0.0046	0.0012	0.001
					0.188
$4p'$ $^2P_{3/2}^{\circ}$	11.693	0.031	0.38	0.095	0.082
$^2P_{1/2}^{\circ}$	11.713	0.011	0.27	0.14	0.138
					0.220
			total	quartets	0.459
				doublets	0.220
					0.679

^a All emission from Cl^* levels below the energy of $\text{Ar}(^3P_2)$ was assigned to excitation by $\text{Ar}(^3P_2)$. Therefore, the channels listed here are not a complete listing for $\text{Ar}(^3P_0)$ and, in fact, the low Cl^* states, especially $\text{Cl}(4s)$, probably have larger rate constants. The experimental uncertainties of these rate constants are determined by the reliability of the radiative branching ratios, see Appendix ; ^b energy defect relative to $E(\text{Ar}^*^3P_0) = 11.723 \text{ eV}$; ^c relative to the rate constant for the favoured channel $5p(^4P_{3/2}) = 1.0$.

constants providing that $\text{Ar}(^3P_0)$ does not specifically favour some particular $\text{Cl}(4p)$ level as an exit channel. The numerous $\text{Cl}(5s)$ and $3d$ levels lying close to the $\text{Ar}(^3P_2)$ entrance channel energy might be the expected products. Unfortunately, transitions from these levels are to the $\text{Cl}(4p)$ manifold or to the Cl ground state ; the former are well into the infrared, while the latter are in the vacuum ultraviolet, and neither were measurable by our apparatus (but see the accompanying paper). The emissions which were observed are from the $4p$ manifold and represent the sum of direct $\text{Cl}(4p)$ excitation and radiative cascade from the $\text{Cl}(5s)$ and $3d$ manifolds to the $\text{Cl}(4p)$ levels.

Table 4 lists the rate constants for formation of the $\text{Cl}(4p)$ levels. These rate constants were obtained by comparing Cl^* emission intensities with Kr^* emission intensities obtained from pre-prepared mixtures of Ar , Cl_2 , Kr for which the % Cl_2 dissociation was measured. Since excitation of Cl^* and Kr^* both arise from $\text{Ar}(^3P_2)$, the concentration ratio, the intensity ratio and the rate constant ² for Kr^* excitation give the Cl^* rate constants. Emissions were observed from all $\text{Cl}(4p)$ levels. Within a given manifold the populations tend to increase with increasing J value (increasing degeneracy factor but lower total energy or larger energy defect). However, no single set of levels was overwhelmingly favoured ; rather, the populations seem to correlate roughly with the degeneracy. The ratio of quartet to doublet emissions is $\sim 5 : 3$, which is reasonably close to the 2 : 1 degeneracy ratio obtained by summing

the degeneracies of the individual levels. This suggests that the Cl(4*p*) levels are mainly produced by direct reaction, since radiative cascade from the 5*s* or 3*d* levels should favour the quartet states because the branching from Cl(3*d* and 5*s*) doublets states would be to the Cl ground state rather than to the Cl(4*p*) levels (see Appendix for further details).

TABLE 4.—RATE CONSTANTS FOR FORMATION OF Cl(4*p*)^a LEVELS FROM (Ar³P₂)^b

level	energy/eV	Δ <i>E</i> /eV ^c	<i>k</i> _{rel} ^d	(<i>k</i> _{rel} / <i>g</i>)	rate constant/ 10 ⁻¹¹ cm ³ molecule ⁻¹ s ⁻¹
4 <i>p</i> ⁴ S _{3/2} ^o	10.629	0.919	0.71	0.18	0.46
4 <i>p</i> ⁴ D _{5/2} ^o	10.401	1.147	0.41	0.051	0.27
⁴ D _{3/2} ^o	10.430	1.118	0.25	0.042	0.16
⁴ D _{1/2} ^o	10.474	1.074	0.29	0.073	0.19
⁴ D _{3/2} ^c	10.499	1.049	0.21	0.11	0.14
					0.75
4 <i>p</i> ⁴ P _{3/2} ^o	10.280	1.268	1.00	0.17	0.65
⁴ P _{1/2} ^o	10.306	1.242	0.42	0.11	0.27
⁴ P _{3/2} ^c	10.335	1.213	0.32	0.16	0.21
					1.13
4 <i>p</i> ² S _{1/2} ^o	10.568	0.980	0.29	0.15	0.19
4 <i>p</i> ² D _{5/2} ^o	10.494	1.054	0.49	0.082	0.32
² D _{3/2} ^o	10.536	1.012	0.52	0.13	0.34
					0.66
4 <i>p</i> ² P _{3/2} ^o	10.592	0.956	0.57	0.14	0.37
² P _{1/2} ^o	10.652	0.896	0.31	0.16	0.20
					0.57
			total	quartets	2.34
				doublets	1.42
					3.76

^a The rate constants for excitation of the Cl(4*s*) levels are reported in the accompanying paper ;
^b these rate constants include both radiative cascade from Cl(5*s* and 3*d*) levels and direct excitation the latter is thought to predominate (see text). The experimental uncertainties in the rate constants are estimated as ± 30 %. Since no corrections need to be made for radiative branching, these values should be more reliable than the values of table 3 ; ^c energy defect relative to $E(\text{Ar}^{*3}P_2) = 11.548$ eV ;
^d relative to the rate constant for the favoured channel $[4p(^4P^3)] = 1.0$.

If the rate constants for formation of Cl(3*d* and 5*s*) levels close to the Ar(³P₂) energy were similar to that for Cl(5*p* and 4*p'*) from Ar(³P₀), radiative cascade would account for ~ 30 % of the emission from Cl(4*p*) levels. The rate constants assigned to Cl(3*d* and 5*s*) from the emission observed in the vacuum u.v.^{4b} also suggests (but does not prove) that direct excitation of (4*p*) dominates over radiative cascade. The most conclusive (and most surprising) result of the vacuum u.v. study was the complete dominance of the Cl(4*s*) exit channel over all other channels, including the excitation to Cl(4*p*).

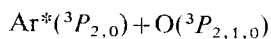


Fig. 3 is an energy level diagram for argon and oxygen atoms. The quenching of Ar(³P_{2,0}) by O atoms previously has been shown to produce O(3*p*³P) directly and O(3*p*⁵P) by collisional cascade.³ The present experiment was concerned only with obtaining a better value for the rate constant for production of O(3*p*³P). The experiments were done at > 1 Torr, which is sufficiently low that only O(3*p*³P) → O(3*s*³S^o) emission at 844.6 nm and not O(3*p*⁵P) → O(3*s*⁵S^o) at 773 nm was observed.

The oxygen atom concentration was determined from measurement of the % O₂ dissociation in a mixture containing helium, oxygen and krypton. The rate constant was deduced from the relative concentrations of Kr and O, the relative Kr* and O* emission intensities, and the rate constant for Ar(³P₂) + Kr. The revised rate constant

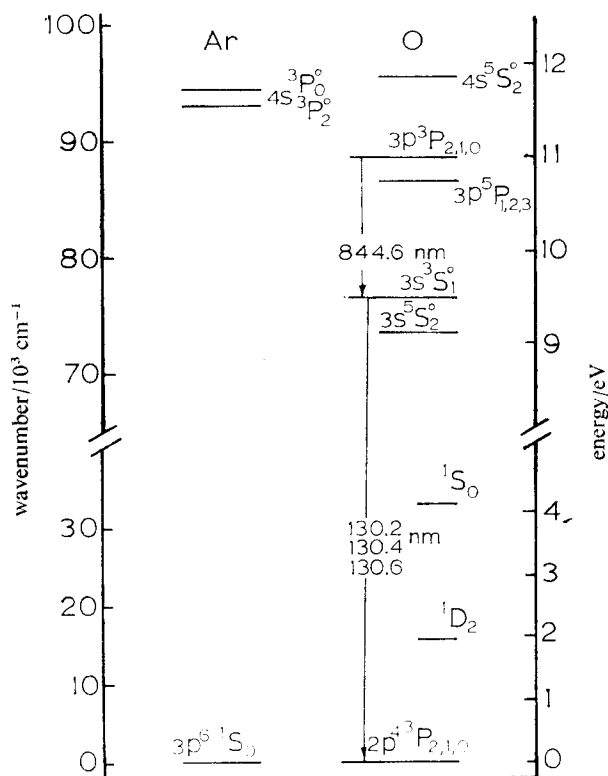


FIG. 3.—Energy level diagram for Ar(³P_{0,2}) and excited states of oxygen atoms. The wavelengths of important transitions are listed in the figure.

for excitation to O(³p³P) is $4.1 \times 10^{-11} \text{ cm}^3 \text{ molecule}^{-1} \text{ s}^{-1}$, which corresponds to a cross-section of 5.5 \AA^2 . The uncertainty in the rate constant, which mainly originates from the determination of [O], is estimated to be better than $\pm 40 \%$.

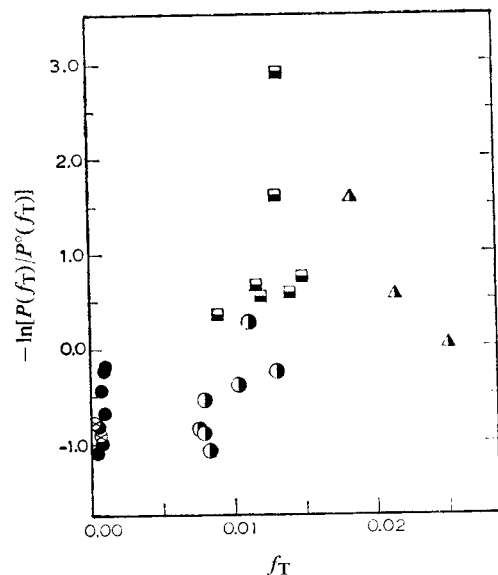
DISCUSSION

Ar(³P_{2,0}) + Xe

The xenon reaction is the simplest example to demonstrate the cumulative effect of a high density of exit channels resulting in a large total quenching rate constant. The number of exit channels is too large for a detailed examination of the interaction between individual entrance and exit channels, and the Xe* distribution will be examined with an emphasis on the validity of a statistical approach. The various *J* states (see tables 1 and 2) within a manifold appear to be populated in approximate accord with the electronic degeneracy; however, the k_{rel}/g values for the *7d* levels from Ar(³P₂) and the *8d* levels from Ar(³P₀) are roughly three to four times larger than for any of the other levels. If the *6f* and the *5f* relative rate constants are

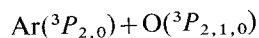
weighted by a Boltzmann factor, $\exp -\Delta E/RT$, to roughly account for collisions that lack sufficient kinetic energy to produce these Xe^* levels, the $7d$ and $8d$ levels are still favoured by about a factor of 2. There is no obvious correlation of rate constant with energy defect for either positive or negative defects, except for the lowest $7d$ and $5d'(\frac{5}{2})_2$ levels from $\text{Ar}(^3P_2)$ and $8d(\frac{3}{2})_1$ level from $\text{Ar}(^3P_0)$. The latter is the only $8d$ level which has a negative energy defect, and it is excited about 25 times less efficiently than the other $8d$ levels.

A systematic way of examining the deviation of product distributions from the completely statistical distribution is provided by a surprisal analysis.⁵⁻⁷ The statistical (prior) distribution is given by $(2J+1)(E_T)^{\frac{1}{2}}$; $(2J+1)$ is the electronic degeneracy and $(E_T)^{\frac{1}{2}}$ is the translational state density per the electronic degeneracy and E_T is the translational state density per unit volume for products with translational energy, E_T . The translational energy of reactants, approximated as $\frac{3}{2}kT$, was included as available energy, since the energy of some final product states exceeded the argon excitation energy. The endoergic products are probably favoured by the high energy tail of the Boltzmann distribution and the $\frac{3}{2}kT$ approximation may be poor for endoergic channels.



do not fit a simple function and, in fact, show opposing dependencies on f_T , *i.e.*, the $7d$ points show a positive slope while the $5d'$ have a negative slope. The data span a very small region of f_T , however, and more complete plot would include the various lower energy states of xenon. On such a plot the data would then show a tendency toward a positive slope, since the population of Xe states for $f_T > 0.03$ is vanishingly small. The surprisal analysis does not provide any particular insight into the $\text{Ar}(^3P_2) + \text{Xe}$ collision processes; disposal of translational energy is apparently not an important aspect of the dynamics.

The broad distribution of Xe^* product states suggests that the strengths of the interactions at the crossing points of the entrance and various exit channel potentials are similar, but some general trends may be deduced. The excitation of exoergic channels can be effected by crossings if the entrance channel is more attractive than the exit channels. This seems to be the case for the d and p exit channels. The very weak excitation of the endoergic $8d(^3\frac{3}{2})_1$ level would tend to support this theory since this d level repulsive exit channel cannot cross with the entrance channel except possibly at short range. On the other hand, the excitation of the endoergic f and s levels tends to indicate that these exit channels are themselves more attractive than the entrance channel. Since the s and f levels and the p levels all have similar excitation probabilities, the crossings may occur at roughly the same place on the entrance channel, namely the repulsive shoulder of the entrance channel. The enhanced excitation of the $7d$ and $8d$ levels relative to the other levels suggests that these crossings are in the potential well of the entrance channel. One other interesting feature is that the $8p[\frac{3}{2}]_2$ and $9p[\frac{3}{2}]_2$ levels are excited much less strongly than any of the other p levels. In homonuclear diatomic rate gas molecules¹⁵ the $p[\frac{3}{2}]_2$ configuration correlates with a fairly strongly bound molecular state in contrast to the other p configurations. If this also is the case for $\text{Xe}^* + \text{Ar}$, the crossing of the potential of the $[\frac{3}{2}]_2$ configuration with the entrance channel will be on the repulsive wall of the entrance channel and hence will be endoergic.



The new experiments confirm Piper's results³ regarding direct formation of $\text{O}(3p^3P)$ with subsequent formation of $\text{O}(3p^5P)$ by collisions between Ar and $\text{O}(3p^3P)$. The thermal cross section for formation of $\text{O}(3p^3P)$ has been revised upward, because of the previous overestimation of the percent O_2 dissociation. The vacuum ultraviolet emission from $\text{O}(3s^3S^0)$ has been observed; however, based upon line width measurements and qualitative comparison with the Kr^* intensity in the vacuum ultraviolet, the direct formation of $\text{O}(3s^3S^0)$ by $\text{Ar}^* + \text{O}$ is less significant than is the contribution from radiative cascade. Further work in which the O^* and Kr^* emission intensities are simultaneously compared in both the visible and in the vacuum ultraviolet is needed to establish definitively the importance of direct production of $\text{O}(3s^3S^0)$. In the following discussion we will assume that $\text{O}(3p^3P)$ is the major exit channel. Since the number of potential curves in the $\text{Ar}^* + \text{O}$ system is relatively small (at least compared to $\text{Ar}^* + \text{Cl}$), and since $\text{Ar}^* + \text{O}$ may serve as prototype for other systems in which an ionic intermediate may be an important mechanism for coupling entrance and exit channels, examination of the potential curves for the $\text{Ar}^* + \text{O}$ system is worthwhile. The mechanism for formation of $\text{O}(3p^3P)$ initially³ was explained by a double curve crossing involving an Ar^+O^- ionic intermediate to connect the entrance and exit channels. However, the analysis below suggests that a direct crossing between a bound $\text{Ar}-\text{O}^*$ entrance channel and the exit channel may be more important.

The simple molecular orbital description¹⁶ will be used to identify and characterize the molecular states. To a first approximation the molecular orbital configurations 2440, 2431 and 2422 correlate with ground state Ar and the three spin orbit states of O; the curves calculated by Dunning *et al.*¹⁷ are shown in fig. 5. The 2341, 1441, 2332 and 1432 configurations correlate with singly charged ions ($\text{Ar}^+ + \text{O}^-$). The

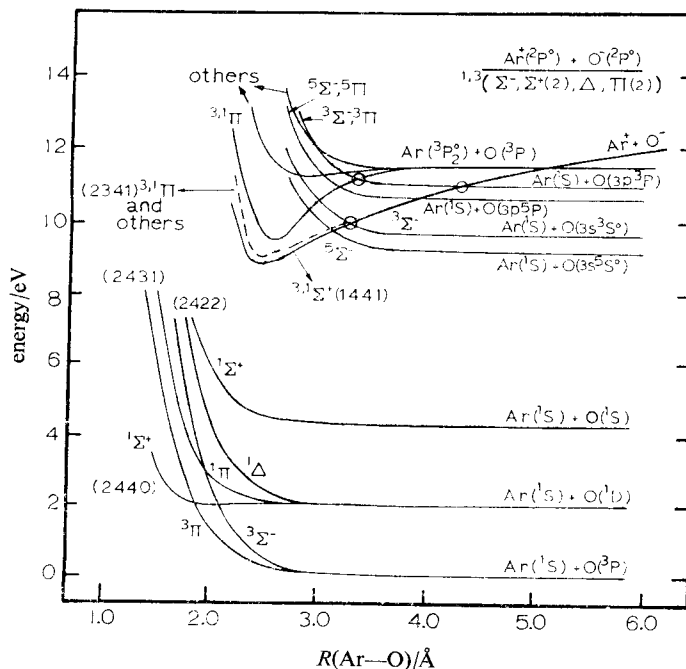


FIG. 5.—Diabatic correlation diagram for $\text{Ar} + \text{O}$. The potential curves correlating with $\text{Ar} + \text{O}(^3P, ^1D, ^1S)$ states were taken from calculations of Dunning *et al.*¹⁷ See the text for procedure used to estimate the other excited state potential curves. The circled crossing points identify states of the same symmetry. The four numbers in the parenthesis identify the molecular orbital description of the core electrons.

lowest energy ion state was estimated using the coulombic attraction at long range, location of the minimum was obtained from the ArO^* emission^{18, 8} assuming that the terminal state of the radiative transition was $^3\Pi(\text{Ar} + \text{O})$; this gives $R_e \approx 2.5 \text{ \AA}$. The 2242, 1342 and 0442 configurations correlate with doubly charged ions ($\text{Ar}^{2+} + \text{O}^{2-}$) and need not be considered for this work. According to Krauss,¹⁹ the lowest ion pair potentials will be the $^1, ^3\Sigma^+$ states corresponding to the 1441 configuration. These are represented by the solid line in fig. 5, and the remaining ion pair curves are collectively represented by the dotted potential curve. In practice the diabatic curves dissociating to singly charged ions actually will be intersected by curves correlating with one ground and one excited state atom; these ionic curves will interact with potentials of appropriate symmetry and may dissociate adiabatically to excited neutrals.

The potential curves for $\text{Ar} + \text{O}(3s)$ were assumed to be similar to potential curves for $\text{Ar} + \text{alkali metal}(\text{Na})$.²⁰ These curves may slightly overestimate the repulsive nature, but they should be approximately correct.¹⁹ The potential curves for $\text{Ar} + \text{O}(3p)$ were drawn in the same way; no distinction was made between the Π

and Σ^- states although the Π curves are presumably less repulsive. These $\text{Ar} + \text{O}^*$ potentials correspond to Rydberg states of $\text{Ar}-\text{O}^*$ at short range.

Some of the molecular states correlating to $\text{Ar}(4s) + \text{O}$ correspond to members of the Rydberg series that terminate with $\text{Ar}^+ - \text{O}$. The $\text{Ar}^+ - \text{O}$ species is isoelectronic with $\text{ClO}(^2\Pi)$ and in molecular orbital terms both have a 2430 configuration. The $\text{ClO}(^2\Pi)$ molecule is strongly bound; $^1 D^\circ(\text{Cl}-\text{O}) = 2.5$ eV and $R_e = 2.7$ Å. Other Rydberg states with different core configurations also correlate with the $\text{Ar}(4s) + \text{O}$ limit; no attempt was made to evaluate the remaining potentials, rather one curve of the repulsive type and another of intermediate character were sketched, collectively to represent the "others". The attractive nature of the intermediate curve may be overemphasized as drawn.

Another Rydberg series can be formed by adding a Rydberg electron to the $2421 (\text{ArO})^+$ core. In this case the Rydberg electron can be localized on the oxygen atom. Although the core assignment is not unique, some of the states generated by a 2421 configuration plus $s(\sigma)$, $p(\sigma)$ and $p(\pi)$ are of the proper symmetry for the $\text{Ar} + \text{O}^*$ states. Thus, the $^3,^5\Sigma^-[\text{Ar} + \text{O}(3s)]$, $^3,^5\Sigma^-[\text{Ar} + \text{O}(3p)]$ and $^3,^5\Pi[\text{Ar} + \text{O}(3p)]$ states arise from the 2421 core plus a $s(\sigma)$, $p(\sigma)$ and $p(\pi)$ Rydberg electron, respectively. The important point is that the $\text{Ar} + \text{O}^*$ states are likely to be less strongly bound than the $^1,^3\Pi[\text{Ar}(4s) + \text{O}]$ entrance channel states.

In order to proceed further with the analysis, the symmetries of the reactant, intermediate and product states must be matched. If we assume a coupling scheme based on Hund's case (a), these symmetries are determined following Herzberg;²² however, consideration of the J value of the initial atomic reactant states will reduce the number of accessible states based on case (a) coupling. For example, $\text{Ar}(^3P_{2,1,0}) + \text{O}(^3P_{2,1,0})$ can produce Σ^+ , $\Sigma^-(2)$, $\Pi(2)$ and Δ states with singlet, triplet and quintet spin multiplicity, but since $\text{Ar}(^3P_1)$ is absent the number of entrance channel states are roughly reduced by 30%. Similarly, $\text{Ar}(^2P^\circ) + \text{O}(^2P^\circ)$ gives Σ^- , $\Sigma^+(2)$, $\Pi(2)$, and Δ states of singlet or triplet multiplicity. Some of these states correlate with ion states of $J = \frac{1}{2}$ rather than $\frac{3}{2}$ and may be less favoured as intermediate channels. If only $\text{Ar}(^3P_2)$ contributes to the reactant channel, the transfer to $V(\text{Ar}^+, \text{O}^-)$ should show some preference for $\text{Ar}(^2P_{3/2})$ over $\text{Ar}(^2P_{1/2})$, because a change of core is required for the latter. This is not true for $\text{O}(^2P_{3/2})$ in contrast with $^2P_{1/2}$, and a statistical distribution of J states is expected for O^- . The $\text{Ar}(^2P_{3/2}) + \text{O}(^2P_{3/2})$ correlate with $^1,^3\Pi$, $^1,^3\Delta$, $^1,^3\Sigma^+$, $^1,^3\Sigma^-$, while $\text{Ar}(^2P_{1/2}) + \text{O}(^2P_{3/2})$ correlate with $^1,^3\Pi$ and $^1,^3\Sigma^+$. The only significant symmetry restriction for the $\text{Ar} + \text{O}^-$ potentials relative to $\text{Ar}(^3P_2) + \text{O}$ is the absence of quintet states. The more attractive $\text{Ar}(4s) + \text{O}$ potentials have singlet and triplet multiplicity. Thus, formation of $\text{O}(3s^3S)$ or $\text{O}(3p^3P)$ is disfavoured from either $V(\text{Ar}^*, \text{O})$ or $V(\text{Ar}^+, \text{O}^-)$, which is consistent with experimental results.

The crossing points of the same symmetry are indicated by circles in fig. 5. Based upon symmetry, two possible mechanisms evidently exist for formation of $\text{O}(3p^3P)$: (i) direct transfer from the bound $^3\Pi[\text{Ar}(4s) + \text{O}]$ entrance potential and (ii) transfer from $^3\Pi$ or $^3\Sigma^-(\text{Ar} + \text{O}^-)$ following the initial transfer from $\text{Ar}(4s)$ to $\text{Ar} + \text{O}^-$. According to the curves drawn for fig. 5, the $^3\Sigma^-(\text{Ar} + \text{O}^-)$ potential should facilitate formation of $\text{O}(3s^3S)$ as a product. Although there may be some direct formation of this state, the current experimental evidence suggests that $\text{O}(3p^3P)$ is more important than $\text{O}(3s^3S)$. If the charge-transfer mechanism is involved for formation of $\text{O}(3p^3P)$, an explanation for the small probability of forming $\text{O}(3s^3S)$ is required. One explanation is the existence of a very strong interaction at the crossing point between the ionic curve and the exit channel producing $\text{O}(3s^3S)$ with a resulting nearly unit probability for adiabatic behaviour which would prevent leakage to the

O(3s) exit channel.* Crossing radii of 3-6 Å are not so large as to discriminate against the charge transfer mechanism;^{2,3} however, changes in core symmetry may reduce the effectiveness of the ionic-intermediate channel for excitation of both O(3s³S) and O(3p³P).

As previously noted, the ³Π[Ar(4s)+O] curve corresponds to a 2430 Ar⁺O core. The ³Π[Ar+O(3p)] and ³Σ⁻[Ar+O(3s)] potentials correspond to a 2421 core. Transfer to the ³Σ⁻ channel from ³Π[Ar(4s)+O] is prohibited by overall symmetry, and this provides a convenient explanation of the experimentally observed low yield of O(3s³S). This also implies that the ³Σ⁻[Ar(4s)+O] component of the entrance channel is sufficiently repulsive that direct crossing with ³Σ⁻[Ar+O(3s)] does not occur. The transfer to ³Π[Ar+O(3p)] is allowed by overall symmetry, although the cores do have different configurations and the transfer requires a two electron process

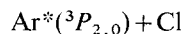
TABLE 5.—Ar(³P₂)+Cl PRODUCT STATE DISTRIBUTION ^a

Cl* level	energy defect/eV	prior distribution P ^o (f _p)	experimental distribution P(f _v)
5s and 3d		0.389	~0.021
4p ⁴ S ^o $\frac{3}{2}$	0.929	0.025	0.019
4p ² S ^c $\frac{1}{2}$	0.98	0.013	0.008
4p ² P ^o $\frac{3}{2}$	0.96	0.026	0.015
$\frac{1}{2}$	0.90	0.013	0.008
4p ² D ^o $\frac{5}{2}$	1.05	0.040	0.013
$\frac{3}{2}$	1.01	0.026	0.014
4p ⁴ D ^o $\frac{7}{2}$	1.15	0.056	0.011
$\frac{5}{2}$	1.12	0.042	0.006
$\frac{3}{2}$	1.07	0.027	0.008
$\frac{1}{2}$	1.05	0.013	0.006
4p ⁴ P ^o $\frac{5}{2}$	1.27	0.045	0.027
$\frac{3}{2}$	1.24	0.024	0.011
$\frac{1}{2}$	1.21	0.015	0.009
4s' ² D $\frac{5}{2}, \frac{3}{2}$	1.12	0.055	0.022
4s ² P $\frac{3}{2}$	2.35	0.040	0.260
$\frac{1}{2}$	2.27	0.020	0.041
4s ⁴ P $\frac{5}{2}$	2.63	0.063	0.102
$\frac{3}{2}$	2.57	0.042	0.413
$\frac{1}{2}$	2.53	0.021	0.020

^a The total product formation rate constant is 2.5×10^{-10} cm³ molecule⁻¹ s⁻¹

for the simple representation used for the states in fig. 5. Formation of ³Σ⁻[Ar+O(3s)] or ³Π[Ar+O(3p)] with a 2421 core from the ³Σ⁻(Ar⁺O⁻) state with 2332 configuration or ³Π(Ar⁺O⁻) with 1432, 2341 or 2332 configurations, requires an extensive change in core configuration and excitation of an oxygen electron to a Rydberg state. The absence of the O(3s³S) as a product and the extensive electron rearrangements required to effect crossing from V(Ar⁺, O⁻) to V(Ar, O*) suggest that the direct curve crossing in the V(Ar*, O) entrance channel may be the favoured pathway for excitation.

* If the interactions between V(Ar⁺, O⁻) and V(O(3s³S), Ar) are estimated by the empirical rules of ref. (24), a strong interaction which approaches the adiabatic limit is suggested. This empirical correlation, however, does not take into account changes in core configuration.



By combining results from the vacuum ultraviolet and the visible emission studies, the Cl* product distribution of table 5 was obtained. The vacuum ultraviolet emissions from the Cl(5s) and Cl(3d) levels were weak;^{4b} however, the relative rate constants of table 5 should be approximately correct. The Ar* + Cl reaction can be summarized as follows:

(1) Formation of $5p^4P^{\circ}$, $5p^4D^{\circ}$, and $4p^2P^{\circ}$ levels occurs with quenching of Ar³P₀ without any strong preference for either quartet or doublet Cl* states. The rate constant for formation of these channels is approximately $0.7 \times 10^{-11} \text{ cm}^3 \text{ molecule}^{-1} \text{ s}^{-1}$. Some of the observed levels are above $E(\text{Ar}, ^3P_0)$ and conversion of translational energy into electronic excitation is required. Lower Cl* levels also are presumably produced but these rate constants could not be assigned because of simultaneous excitation by Ar(³P₂), which is present in seven fold excess.

(2) Quenching of Ar(³P₂) gives the 5s, 3d, and 4p levels; the relative rate constants are not firmly established but the 5s and 3d levels appear to be less strongly populated than are the Cl(4p) levels. The observed rate constant (direct formation plus radiative cascade) for Cl(4p) is $3.8 \times 10^{-11} \text{ cm}^3 \text{ molecule}^{-1} \text{ s}^{-1}$. There was no strong preference for quartets, doublets or for particular *J* states among the 4p levels.

(3) The most remarkable feature about the Ar(³P₂) + Cl reaction was discovered by Nip and Clyne^{4b} from the vacuum ultraviolet emissions. In addition to the weak emissions from Cl(3d, 5s and 4s'), extremely strong emissions were observed from the Cl(4s ⁴P_{*J*} and ²P_{*J*}) states. The rate constant for emission from these levels is $\sim 2.0 \times 10^{-10} \text{ cm}^3 \text{ molecule}^{-1} \text{ s}^{-1}$, far too large to be the result of radiative cascade from upper levels; without doubt these Cl(4s) levels are directly produced by two-body quenching. Within the Cl(4s) manifold the $J = \frac{3}{2}$ states are strongly favoured and the $J = \frac{1}{2}$ states strongly unfavoured.

(4) The total quenching rate constant is $2.4 \times 10^{-10} \text{ cm}^3 \text{ molecule}^{-1} \text{ s}^{-1}$ and $\sim 85\%$ of the products are the Cl(4s) states. Direct formation of Cl(4p) levels with energy defects of $\sim 1 \text{ eV}$ was surprising, but the 2.5 eV defect for the Cl(4s) levels is enormous.

In order to emphasize the favouring of exit channels with large energy defects, the data are presented on a surprisal plot in fig. 6. Since the distributions within the Cl(5s) and Cl(3d) manifold were not measured and since there was no strong preference for *J* within the Cl(4p) levels, the relative populations were summed over all *J* of the same term symbol. With this simplification, a strong trend emerges and channels with larger energy defects are clearly favoured, even relative to the statistical expectation. The product distribution from the reaction¹ of Hg(³P₁) with Na also is displayed in fig. 6. This reaction exhibits the preference for exit channels with small energy defects that is frequently found for metal atom excitation transfer reactions.^{24, 25} The product distribution from the Ar* + Xe reaction lies between these two clear-cut trends.

In order to explain the Ar(³P₂) + Cl results, a schematic potential energy diagram will be considered. The curves are based upon the same reasoning used for constructing the Ar + O figure. The ²Σ⁺ and ²Π_{*1,2*} ArCl molecular states correlating to the ground atomic states are not of interest to this discussion and are not shown. The coulombic Ar⁺Cl⁻ states are simpler than for Ar⁺O⁻ and have only ²Σ⁺ and ²Π_{*1,2*} symmetry. For simplicity these are shown as a single potential curve, although in fact these will be separated at short range. Recent calculations for KrF²⁶ order the states as ²Σ⁺(Ω = $\frac{1}{2}$), ²Π(Ω = $\frac{3}{2}$) and ²Π(Ω = $\frac{1}{2}$). The $V(\text{Ar}^+\text{Cl}^-)$ shown in fig. 7 is drawn for the KCl Rittner potential²⁷ adjusted to the Ar⁺ + Cl⁻ asymptotic limit.

This potential gives close agreement with the energy separation between the lowest Ar^+Cl^- and the ground $\text{Ar}+\text{Cl}$ state.⁸ The configurations of the ion pair states are 1442 and 2342. The $\text{Ar}+\text{Cl}^*$ Rydberg states are very numerous; we have assumed that the potentials for these are similar to that for $\text{Ar}+\text{alkali metal(K)}$ atoms,²⁰ and have shown these potentials for three representative exit channels in fig. 7. At shorter range the Rydberg ($\text{Ar}+\text{Cl}^*$) states of different symmetry presumably will have unequal repulsion and will separate into a very large number of potential curves.

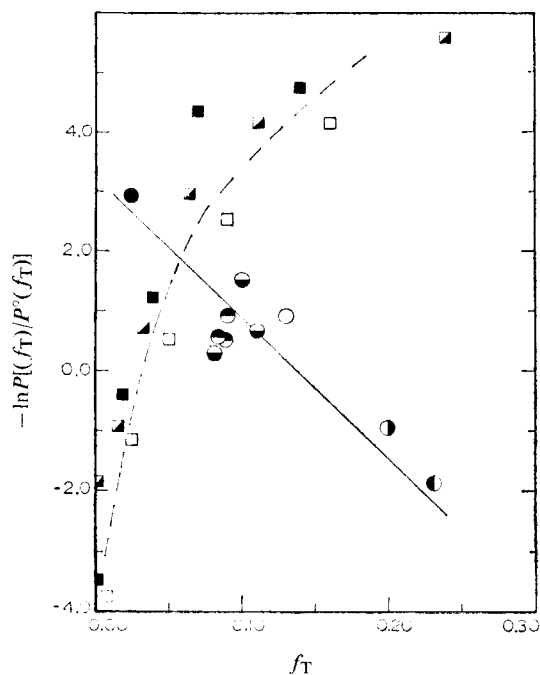


FIG. 6.—Surprisal plot of product states from $\text{Ar}(^3P_2)+\text{Cl}$ (\circ) and $\text{Hg}(^3P_1)+\text{Na}$ (\square).¹ Populations from all J states of a given term were summed in making this plot. The $\text{Na}^*(f)$ levels were not experimentally observed,¹ but are likely products. The Na^* levels with energies in excess of $E(\text{Hg}^3P_1)+\frac{3}{2}RT$ were not included on this plot. Na^* : \square s , \blacksquare p , \blacksquare d . Cl^* : \bullet $3d, 5s$; \circ $4p$ doublet; \ominus $4p$ quartet; \bullet $4s$ doublet; \ominus $4s$ quartet; \circ $4s'$ doublet.

With the exceptions noted below, these will be mainly repulsive in nature. The exception may be curves correlating to $\text{Cl}(4s' ^2D)$, which should be similar to those shown for $\text{Ar}+\text{O}(^1D)$ in fig. 5, since (2431) also is the core configuration of the $\text{Ar}+\text{Cl}^*(4s')$ states. All of the other $\text{Ar}+\text{Cl}^*$ states will have cores that are the same as $\text{Ar}+\text{O}(^3P)$, which are (2431) and (2422) configurations yielding $^3\Pi$ and $^3\Sigma^-$ core states, respectively. The potentials for the entrance channel were estimated by analogy to those for Cl_2 ,²⁸ which is isoelectronic with $\text{Cl}-\text{Ar}^*$. Thus these potentials were viewed as a $\text{Cl}-\text{Ar}^+$ core plus a $s(\sigma)$ Rydberg electron, which has little effect on the core potential curve. The potentials shown are $^1\Sigma^++s(\sigma)$, $^1,^3\Pi+s(\sigma)$, and "others", the latter representing the remaining repulsive potentials that correlate with the entrance channel. The separation between the various $^3\Pi$ curves of Cl_2 is too small to be apparent on the scale of this diagram. The core configurations of the bound entrance channels are 2440 and 2431.

Although fig. 7 is only qualitative, hopefully it will suffice for discussing and possibly explaining the main features of the Cl^* product distribution. Additional

information⁸ is that emission from Cl(4s) levels is observed from reactions of Ar(³P_{0,2}) with chlorine containing molecule (RCl), whenever these exit channels are energetically allowed. Furthermore, the *J* state distributions from the Ar(³P_{2,0}) + RCl reactions were very similar to those observed here from Ar(³P_{0,2}) + Cl. For the Ar* + RCl reactions it has been suggested that ArCl* molecules initially are formed in high vibrational states and that Cl(4s) is formed by predissociation of the ArCl* with sufficient energy to reach the crossing points between *V*(Ar⁺, Cl⁻) and

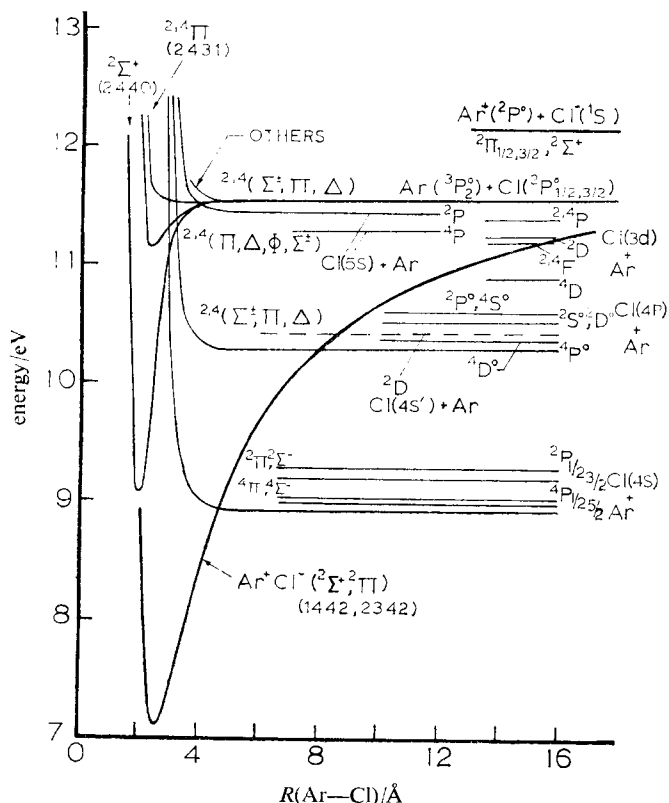


FIG. 7.—Diabatic correlation diagram of the potentials for Ar + Cl. The potential curves correlating to ground states are not shown. The ion pair potential, shown by the heavy line, is the Rittner potential for KCl, which gives nearly the correct wavelength of the ArCl* excimer emission. The ²Σ⁺ and ²Π coulombic states will be separated at short range, but this is not shown. The Rydberg states correlating to Ar + Cl* are assumed to be repulsive and were represented by the Ar-K potential. Only three of the many possible potentials are shown although the total exit channel states, in case (a) coupling, are listed for each grouping of Cl* states. The bound Rydberg potentials correlating to Cl + Ar* were taken to be the same as those for the isoelectronic Cl₂ molecule; an additional "others" potential was added to represent the repulsive potentials of the entrance channel.

V[Ar, Cl(4s)]. Since spin is not a well defined quantum number, interaction between ²Π or ²Σ (Ar⁺ + Cl⁻) and ⁴Σ⁺ or ⁴Π [Ar + Cl(4s)] can occur. A similar explanation must hold for the direct Ar* + Cl reaction, and the question of why the Cl(4s) states are favoured can be replaced by how does the two-body Ar* + Cl collision ultimately sample the *V*(Ar⁺, Cl⁻) potential.

The outer crossing of the entrance channel and *V*(Ar⁺, Cl⁻) occurs at very long range and interaction between the potential curves is negligibly weak. Thus the

interactions of the inner turning points of the curves must be examined. The repulsive limbs of the $V(\text{Ar}^+, \text{Cl}^-)$ potentials are not well established; however, they may closely approach either or both of the $^2\Sigma^+$ or $^2\Pi$ entrance channel potentials, and transfer to $V(\text{Ar}^+\text{Cl}^-)$ from one of these appears to be possible. The strong favouring of the $J = \frac{3}{2}$ states of $\text{Cl}(4s)$ suggests that the interactions may be between $V(\text{Ar}^+, \text{Cl}^-)$ and the $^2,4\Pi$ rather than the $^2\Sigma^+$ entrance channel potentials. After transfer to the ion pair potential, formation of $\text{Cl}(4s)$ occurs via the crossing between $V(\text{Ar}^+, \text{Cl}^-)$ and $V[\text{Ar} + \text{Cl}(4s)]$. The crossing points for formation of $\text{Cl}(4p)$ occurs at larger internuclear distances; hence, the strength of the interactions are weaker and the probability of $\text{Cl}(4p)$ formation is reduced.

A second general question is why are the $\text{Cl}(5s)$ and $3d$ states so weakly populated by the direct reaction. For comparison the rate constants for formation of the Xe^* states close to the entrance channel are an order of magnitude larger. Examination of fig. 7 shows no obvious symmetry restrictions. The relative slopes of the $^2\Sigma^+$ and $^2,4\Pi$ entrance and the $\text{Cl}^* + \text{Ar}$ exit channel curves are very unfavourable; however, within the limitation of our present knowledge it is surprising that an effective interaction does not exist between some of the $3d$ and $5s$ potentials and the entrance channels represented by "others". One possibility (but unproven) is that the "others" are more repulsive than the $4s$ and $3d$ exit channels so that the crossing point is not energetically allowed at room temperature. Another significant factor may be that the exit channel cores are 2422 and 2431, configurations, wherein the core configuration of the "others" are mainly 2341. Thus the coupling at the crossing would involve change of Rydberg state and change of core configuration.

CONCLUSIONS

The reactions of $\text{Ar}(^3P_2)$ with Xe , Cl and O atoms have large excitation transfer rate constants (18×10^{-11} , 25×10^{-11} and 4.1×10^{-11} $\text{cm}^3 \text{ molecule}^{-1} \text{ s}^{-1}$, respectively) and product distributions which do not exhibit the usual decline with increasing energy defect. Such product distributions are in strong contrast to most other atom-atom excitation transfer studies (usually involving metal atoms). The Xe^* product distribution showed little dependence on energy defect, within the observed 0.25 eV range. The $\text{Ar}^* + \text{Xe}$ entrance channel potentials vary from repulsive to mildly attractive, and the crossings with the repulsive exit channels occur at approximately the same position in the entrance channel. Thus large energy defects are not feasible. The product distributions from $\text{Ar}(^3P_2) + \text{Cl}$ and O are surprisingly specific and channels with large energy defects are favoured. Examination of qualitative potential curves for these two cases suggests the importance of strongly attractive potentials in the entrance channel arising from chemical bonding between the non-closed shell reactants. Curve crossing from these bound potentials to exit channels lying well below the entrance channel energy can lead to products. All three of the $\text{Ar}(^3P_{0,2})$ quenching reactions generally involve two electron processes at the crossing points of the potentials. This may provide important selectivity in some instances but certainly does not provide any general inhibition for excitation transfer. Metal atom excitation transfer systems, *e.g.*, $\text{Hg}^* + \text{Na}$,¹ usually favour product states with small energy defects. However, exit channels with large energy defects were observed from $\text{Hg}^* + \text{Na}$,¹ which shows that attractive entrance channel potentials are present. The explanation for the weak coupling to the channels with large energy defects may be that the $V(\text{Na}^* - \text{Hg})$ potentials are quite repulsive. Thus, the exit channel potentials with large energy defects would have unfavourable slopes in the region of crossing with the entrance channels.

This work was supported by the U.S. Army Research Office-Durham and by Donors of the Petroleum Research Fund (administered by the American Chemical Society). We thank Dr. Dunning (Los Alamos Scientific Labs) for permission to use his Ar-O potential curves and Dr. Krause (NBS, Washington) for his comments on an initial draft of the manuscript. We also thank Dr. Jack Davis (NRL, Washington) for the branching ratio calculations for the Cl* levels.

APPENDIX

CALCULATION OF BRANCHING RATIOS

For both the Ar*+Xe and Ar*+Cl systems it was necessary to account for emissions which were not observed before assigning formation rate constants for various levels. Neglect of such emissions would result in underestimation of the formation rate constants.

The transition probability for a radiative transition is given by ²⁹

$$A_{21} = \frac{2.02 \times 10^{15}}{g_2 \lambda^3} S_{21},$$

where S_{21} is the absolute line strength (in atomic units), g_2 the degeneracy of the upper level and λ is the wavelength in nm. The absolute line strength, S_{21} , can be approximated as a product, $S_R \zeta$, where S_R is a relative line strength, independent of the principal quantum number n , and ζ is the square of the reduced matrix element, a function of the orbital angular momentum and radial wave functions of the states involved in the transition. This latter quantity can be calculated from the coulomb approximation of Bates and Damgaard.²⁹ This approximation is generally considered valid for the case of an excited electron in a shell by itself, where the exchange forces are small; thus, transitions terminating in the ground states of Xe or Cl cannot be treated in this approximation. The relative line strength, S_R , is dependent upon the assumed coupling scheme. For Xe, the J_c-1 or Racah scheme has been used, and for Cl Russell-Saunders L-S coupling was utilized.

XENON

The xenon emissions were generally observed from a given upper state to different levels of only one set of radiatively-allowed lower configurations (*e.g.*, $7d \rightarrow 6p$, but not $7d \rightarrow 7p$, $7d \rightarrow 8p$, $7d \rightarrow 4f$, or $7d \rightarrow 6p'$). In the J_c-1 coupling scheme, S_R has been calculated by Faust and McFarlane¹⁴ and also by Statz *et al.*^{11b} Since this quantity is independent of n , relative branching ratios to configurations differing only in the principal quantum number (*e.g.*, $7d \rightarrow 6p$, $7d \rightarrow 7p$, $7d \rightarrow 8p$) depend only on relative values of $\zeta/\lambda^3 (= \Gamma)$. To obtain approximate relative branching ratios to these configurations, an average transition wavelength based on the difference of the statistically averaged energies of upper and lower configurations was used. The average Γ values were then calculated in the Coulomb approximation using average effective quantum numbers. This averaging method was checked with "exact" coulomb calculations for a few transitions, and in most cases was found to be accurate within 20%. A similar method of averaging using only relative Γ values was used for transitions to lower configurations of different orbital quantum number l (*e.g.*, $7d \rightarrow 4f$). Exact calculations showed this method to be less accurate (only within a factor of 2), but was taken to be adequate since in general these latter transitions comprised only a small fraction of the total transition probability. The initial populations of the product channels were then multiplied by the ratio of the sum of all calculated Γ values to the Γ value for the observed transition. This method does not include transitions involving states of different core configuration (primed states). If such transitions are important then our assigned relative populations will be in error. The most important possibilities are the $7d$ and $8d \rightarrow 6p'$ transitions and all transitions from the $5d'$ configuration. Table 6 lists the branching ratios used in the calculations.

Several $5f \rightarrow 5d$ transitions were too far to the red to be measured by our apparatus. For this case, a complete set of "exact" $5f \rightarrow 5d$ transition probabilities were calculated to

ascertain if any significant transitions had been missed. Over 85 % of the important transitions were observed except for transitions from the $5f(\frac{5}{2})_2$ level. The intensity of this level was increased by a factor of 3.3 to include unobserved emissions.

TABLE 6.—AVERAGE BRANCHING RATIOS FOR TRANSITIONS BETWEEN Xe MANIFOLDS

lower configuration	6f	8d	10s	upper configuration 9p	5f	7d	9s	8p
5f		0.036						
4f		0.021				0.029		
8d	0.022							
7d	0.007			0.021	0.034			
6d	0.047			0.156	0.051			0.182
5d	0.924			<0.001	0.915			0.103
9p		0.001	0.149					
8p		0.074	0.141			0.002	0.230	
7p		0.186	0.248			0.186	0.265	
6p		0.684	0.469			0.775	0.505	
9s				0.188				
8s				0.100				0.239
7s				0.098				0.145
6s				0.248				0.332

CHLORINE

For transitions to levels other than ground state chlorine, the Coulomb approximation in the L-S coupling scheme was employed. In this case the relative line strength factor S_R is a product of angular terms $S(L)S(M)$, both of which are tabulated.³⁰

Table 7 lists the results of the calculations for branching from the $5p$ and $4p'$ chlorine levels, populated by quenching of $\text{Ar}(^3P_0)$. The observed emissions were to the $4s$ levels, and corrections were made for unobserved transitions to the $5s$, $3d$ and $4s'$ levels of the same

TABLE 7.—CALCULATED BRANCHING RATIOS FOR Cl $5p$,^a $4p'$ TRANSITIONS

term	J-value	$A_{ki} \times 10^{-8}(\text{obs})^b$	$A_{ki} \times 10^{-8}(\text{unobs})^c$	$A_{ki} \times 10^{-8}(\text{total})$
$5p \ ^4P^\circ$	5	0.013	0.059	0.072
		0.015	0.058	0.073
$5p \ ^4D^\circ$	3	0.031	0.069	0.100
		0.035	0.069	0.104
$4p' \ ^2P^\circ$	2	0.004	0.046	0.050
		0.002	0.043	0.045

^a The ratio of the observed to unobserved branching ratios for the $^4P_{3/2}^\circ$ and $^4D_{3/2}^\circ$ states were taken as the mean of the two entries of the table for these terms. The rate constant for formation of the endoergic $^4P_{3/2}^\circ$ and $^4D_{3/2}^\circ$ states is so small that a large change in the branching ratio will not be significant; ^b to the $\text{Cl}(4s)$ states of the same multiplicity; ^c to the $\text{Cl}(5s)$, $\text{Cl}(3d)$ and $\text{Cl}(4s')$ states of the same multiplicity.

spin multiplicity. The unobserved transition probabilities still represent a lower limit, since no allowance was made for $\Delta S \neq 0$ transitions. Although the observed $5p$ emission was stronger than that of $4p'$, the calculated branching ratios suggest that this may be due to unequal branching, with actual populations more nearly equal. However, this must be tempered by any (but unknown) effects on transitions caused by a change in core configuration, *i.e.*, primed \rightleftharpoons unprimed transitions.

A small number of calculations were made for transitions terminating on the ground state of Cl from Cl $5s$ and $3d$ levels. These calculations, which were supplied by Dr. Jack

Davis, utilized semi-empirical excited wavefunctions and Clementi-Hartree-Fock ground state wavefunctions. The purpose of these calculations was to determine the strength of emission from various Cl $5s$ and $3d$ doublet levels to the $3p^5$ ground state of chlorine, as compared with emission to the $3p^4 4p$ levels. Table 8 demonstrates the overwhelming

TABLE 8.—CALCULATED BRANCHING RATIOS FOR Cl $3d$, $5s$ TRANSITIONS

transition	λ/nm	$A_{ki} \times 10^{-8}$
$3p^4 3d(^2P_{3/2}) \rightarrow 3p^5(^2P_{3/2})$	108.8	4.12
$3p^4 3d(^2P_{1/2}) \rightarrow 3p^4 4p(^2P_{3/2})$	1546.5	0.094
$3p^4 5s(^2P_{3/2}) \rightarrow 3p^5(^2P_{3/2})$	108.0	5.64
$3p^4 5s(^2P_{1/2}) \rightarrow 3p^4 4p(^2P_{3/2})$	1396.0	0.180
$3p^4 5s(^4P_{3/2}) \rightarrow 3p^4 4p(^4P_{3/2})$	1243.0	0.241

preponderance of emission to the ground state for the doublet manifold. The branching for the $5s$ and $3d$ quartet states could not be calculated, but the strength of $\Delta S \neq 0$ transitions from the $4s$ quartet states suggests that changes in spin multiplicity can occur, and the quartet levels may also branch strongly to the ground state. Therefore the majority of the emission from the Cl($4p$) levels probably results from direct $\text{Ar}^+ + \text{Cl}$ excitation rather than cascade from higher Cl* levels. Certainly for the Cl($4p$) doublet states this is the case.

¹ M. Czajkowski, L. Krause and G. Skardis, *Canad. J. Chem.*, 1973, **51**, 334, 1582.

² L. G. Piper, D. W. Setser and M. A. A. Clyne, *J. Chem. Phys.*, 1975, **63**, 5018.

³ L. G. Piper, *Chem. Phys. Letters*, 1974, **28**, 276.

⁴ (a) D. L. King and D. W. Setser, the quenching of $\text{Ar}(^3P_{0,2})$ by Cl atoms and the relationship to the ArCl^* upper state potential was initially discussed at the St. Louis Laser Conference (1974); see *I.E.E.E. J. Quant. Electronics*, 1975, **QE-11**, 708; (b) W. Nip and M. A. A. Clyne, *J.C.S. Faraday II*, 1977, **73**, 161; (c) L. G. Piper and M. A. A. Clyne, personal communication.

⁵ (a) R. B. Bernstein and R. D. Levine, *Adv. Atomic Mol. Phys.*, ed. D. R. Bates (Academic Press, New York, 1975), vol. 11; (b) R. D. Levine and R. B. Bernstein, *Modern Theoretical Chemistry*, ed. W. H. Miller (Plenum Press, New York, 1975), vol. 3; (c) R. D. Levine and R. B. Bernstein, *Accounts Chem. Res.*, 1974, **12**, 393.

⁶ D. J. Bogan and D. W. Setser, *J. Chem. Phys.*, 1975, **64**, 586.

⁷ (a) M. Bubinson and J. I. Steinfeld, *Chem. Phys.*, 1974, **4**, 467; (b) I. Procaccia and R. D. Levine, *J. Chem. Phys.*, 1975, **62**, 3819; (c) R. B. Bernstein, *J. Chem. Phys.*, 1975, **62**, 4570.

⁸ L. Gundel, D. W. Setser, M. A. A. Clyne, J. A. Coxon and W. Nip, *J. Chem. Phys.*, 1976, **64**, 4390. The coefficient in eqn (4) should be 0.31 rather than 0.36; the correct Kr* branching ratios are given in ref. (2) above. The rate constants were calculated with the correct branching ratios.

⁹ W. C. Richardson and D. W. Setser, *J. Chem. Phys.*, 1973, **58**, 1809.

¹⁰ A. R. Striganov and N. S. Sventitskii, *Tables of Spectral Lines of Neutral and Ionized Atoms* (Plenum Press, New York, 1968).

¹¹ (a) Personal communication from L. Allen; (b) H. Statz, C. L. Tang and G. F. Koster, *J. Appl. Phys.*, 1963, **34**, 2625; (c) Ya. F. Verolainen and A. L. Osheroovich, *Optics Spectr.*, 1969, **27**, 14; (d) C. Y. Chen and R. H. Garstang, *J. Quant. Spectr. Rad. Trans.*, 1970, **10**, 1347; (e) M. H. Miller, R. A. Roig and R. D. Bergston, *Phys. Rev. A*, 1973, **8**, 480; (f) C. C. Davis and T. A. King, *J. Quant. Spectr. Rad. Trans.*, 1973, **13**, 825; (g) E. Jimenez, J. Campos and C. Sanchez del Rio, *J. Opt. Soc. Amer.*, 1974, **64**, 1009.

¹² L. G. Piper, J. E. Velazco and D. W. Setser, *J. Chem. Phys.*, 1973, **59**, 3323.

¹³ L. Allen, D. G. C. Jones and D. G. Schofield, *J. Opt. Soc. Amer.*, 1969, **59**, 842.

¹⁴ W. L. Faust and R. A. McFarlane, *J. Appl. Phys.*, 1964, **35**, 2010.

¹⁵ R. S. Mulliken, *J. Chem. Phys.*, 1970, **52**, 5170.

¹⁶ R. S. Mulliken, *J. Chem. Phys.*, 1971, **55**, 288.

¹⁷ T. H. Dunning, Jr., P. J. Hay and R. C. Raffanetti, personal communication.

¹⁸ M. F. Golde and B. A. Thrush, *Chem. Phys. Letters*, 1974, **29**, 486.

¹⁹ M. Krauss, personal communication.

²⁰ U. Buck and H. Pauly, *Z. Phys.*, 1968, **208**, 390.

²¹ P. A. G. O'Hare and A. C. Wahl, *J. Chem. Phys.*, 1971, **54**, 3770.

- ²² G. Herzberg, *Molecular Spectra and Molecular Structure I. Spectra of Diatomic Molecules* (Van Nostrand, Princeton, 1961), p. 318.
- ²³ (a) R. Grice and D. R. Herschbach, *Mol. Phys.*, 1974, **27**, 159; (b) J. C. Hasted and A. Y. J. Chong, *Proc. Phys. Soc.*, 1962, **80**, 441; (c) R. E. Olson, F. T. Smith and E. Bauer, *Appl. Optics*, 1970, **10**, 1848.
- ²⁴ L. Krause, *Adv. Chem. Phys.*, 1975, **28**, 267.
- ²⁵ D. L. King and D. W. Setser, *Ann. Rev. Phys. Chem.*, 1977, **28**, in press.
- ²⁶ T. H. Dunning, Jr. and P. J. Hay, *Appl. Phys. Letters*, 1976, **28**, 649.
- ²⁷ P. Brummer and M. Karplus, *J. Chem. Phys.*, 1973, **58**, 3903.
- ²⁸ J. A. Coxon, *Molecular Spectroscopy—Volume 1*, (Specialist Periodical Report, The Chemical Society, 1973), p. 177.
- ²⁹ D. R. Bates and A. Damgaard, *Phil. Trans. Roy. Soc. A*, 1949, **242**, 101.
- ³⁰ B. W. Shore and D. H. Menzel, *Astrophys. J. Supp. Ser.*, 1965, **12**, 187.

(PAPER 6/895)